The Astronomical Journal, 132:2296–2308, 2006 December
© 2006. The American Astronomical Society. All rights reserved. Printed in U.S.A.

NICMOS2 *HUBBLE SPACE TELESCOPE* OBSERVATIONS OF THE EMBEDDED CLUSTER ASSOCIATED WITH MON R2: CONSTRAINING THE SUBSTELLAR INITIAL MASS FUNCTION

M. Andersen, M. R. Meyer, and B. Oppenheimer
Steward Observatory, University of Arizona, 933 North Cherry Avenue, Tucson, AZ 85721;
mandersen@as.arizona.edu, mmeyer@as.arizona.edu

C. Dougados
Laboratoire d'Astrophysique de Grenoble, Grenoble Cedex 9, France

and

J. Carpenter
Department of Astronomy, California Institute of Technology, Pasadena, CA 91125
Received 2006 March 3; accepted 2006 July 30

ABSTRACT

We have analyzed *Hubble Space Telescope* NICMOS2 F110W-, F160W-, F165M-, and F207M-band images covering the central $1' \times 1'$ region of the cluster associated with Mon R2 in order to constrain the initial mass function (IMF) down to $20M_J$. The flux ratio between the F165M and F160W bands was used to measure the strength of the water-band absorption feature and select a sample of 12 out of the total sample of 181 objects that have effective temperatures between 2700 and 3300 K. These objects are placed in the H-R diagram together with sources observed by Carpenter et al. to estimate an age of $\sim$1 Myr for the low-mass cluster population. By constructing extinction-limited samples, we are able to constrain the IMF and the fraction of stars with a circumstellar disk in a sample that is 90% complete for both high- and low-mass objects. For stars with estimated masses between 0.1 and 1.0 $M_\odot$ for a 1 Myr population with $A_V \leq 19$ mag, we find that 27% $\pm$ 9% have a near-infrared excess indicative of a circumstellar disk. The derived fraction is similar to or slightly lower than the fraction found in other star-forming regions of comparable age. We constrain the number of stars in the mass interval 0.08–1.0 $M_\odot$ to the number of objects in the mass interval 0.02–0.08 $M_\odot$ by forming the ratio $R^{**} = N(0.08\text{–}1\ M_\odot)/N(0.02\text{–}0.08\ M_\odot)$ for objects in an extinction-limited sample complete for $A_V \leq 7$ mag. The ratio is found to be $R^{**} = 2.2 \pm 1.3$, assuming an age of 1 Myr, consistent with the similar ratio predicted by the system IMF proposed by Chabrier. The ratio is similar to the ratios observed toward the Orion Nebula Cluster and IC 348, as well as the ratio derived in the 28 deg^2 survey of Taurus by Guieu et al.

Key words: open clusters and associations: individual (Mon R2) — stars: formation — stars: low-mass, brown dwarfs — stars: luminosity function, mass function — stars: pre–main-sequence

Online material: machine-readable table

1. INTRODUCTION

The shape of the initial mass function (IMF) and whether it is universal have been central questions in astrophysics for more than 50 years. The shape of the stellar part of the IMF has been examined observationally in some detail. Above 0.5 $M_\odot$, the IMF derived for field stars is well characterized by a Salpeter power law, $dN/dM \propto M^{-\alpha_1}$, $\alpha_1 = 2.35$ (Kroupa 2002). At this characteristic mass, the slope of the power law changes to $\alpha_2 = 1.35$, and for masses below 0.1 $M_\odot$ the IMF flattens further (Kroupa 2002; Chabrier 2003), although the slope is very uncertain (Allen et al. 2005). To search for variations in the IMF as a function of environment, one has to look at individual star-forming episodes, such as star clusters or associations. Young clusters in particular are useful for these studies because the more massive stars are still present in the cluster and the clusters have not experienced significant dynamical mass segregation. Recently, the IMF studies have been extended deep into the brown dwarf regime in several star-forming regions, most notably the Orion Nebula Cluster (ONC; e.g., Hillenbrand & Carpenter 2000; Muench et al. 2002; Slesnick et al. 2004), IC 348 (e.g., Najita et al. 2000; Luhman et al. 2003), and Taurus (e.g., Briceño et al. 2002; Luhman 2004; Guieu et al. 2006).

In order to search for variations in the substellar IMF as a function of environment, a larger ensemble of young clusters is needed. Here we present a study of the IMF in the Mon R2 cluster. The embedded cluster associated with Mon R2 was originally discovered by Beckwith et al. (1976) and is located at a distance of 830 $\pm$ 50 pc (Herbst & Racine 1976). The most massive star in the cluster is $\sim$10 $M_\odot$ (Carpenter et al. 1997; Massi et al. 1985). Carpenter et al. (1997) estimated Mon R2 to contain at least 475 stars within a 3.6 pc $\times$ 3.6 pc region, significantly less than the $\sim$3500 stars found within a 2.5 pc radius of the ONC (Hillenbrand & Hartmann 1998). IC 348 contains $\sim$400 members, including brown dwarfs (Luhman et al. 2003). Thus, Mon R2 has a richness intermediate between the two well-studied clusters. The molecular cloud has been shown by Choi et al. (2000) to have a central density of $n_c \sim 10^7$ cm^{-3}, much higher than typical densities in the Taurus molecular cloud cores ($n_c \sim 10^5$ cm^{-3}; see, e.g., Onishi et al. 2002). If the densities of the molecular cores have an impact on the IMF as suggested by, e.g., Bate & Bonnell (2005) and Goodwin et al. (2004a), we would expect the IMF in Mon R2 to have relatively more brown dwarfs than Taurus.

Previously, Carpenter et al. (1997) imaged Mon R2 down to the brown dwarf limit and obtained spectra for a subset of the stars. They established that the age of the cluster was $\leq$3 Myr

and that the majority of the low-mass stars clustered around the 1 Myr isochrone. Adopting an age of 1 Myr for the stellar population, they found the ratio of high-mass to low-mass stars, $N(1\text{–}10\ M_\odot)/N(0.1\text{–}1\ M_\odot) = 0.1$, which is consistent with other nearby star-forming regions (Meyer et al. 2000) and with a Miller & Scalo (1979) field star IMF. Despite the fact that Mon R2 is relatively nearby, the brown dwarf content has not been investigated in a systematic manner. Here we present *Hubble Space Telescope* (*HST*) NICMOS2 near-infrared imaging of the central 0.24 pc × 0.24 pc ($1' \times 1'$) of the cluster. Our main goal is to constrain the low-mass stellar and brown dwarf content in the cluster and compare the results to those derived for other young clusters and the field. In addition, we estimate the fraction of stars with disks within our surveyed region.

The paper is structured as follows: In § 2 we present the observations, the data reduction, and the photometry. Section 3 presents the results from the color-magnitude and color-color diagrams for the cluster. We place objects in the H-R diagram based on the estimate of the effective temperature derived from the F160W- and F165M-band observations. In § 4 we discuss our constraints on the IMF and disk frequency based on extinction-limited samples constructed from our observations. Section 5 compares our derived ratios with the similar ratios for other star-forming regions. Finally, we conclude in § 6 with a summary of our results.

2. OBSERVATIONS AND REDUCTION

2.1. *The Data Set*

HST NICMOS2 observations of the central $1' \times 1'$ of Mon R2 were obtained in Cycle 7 under program number 7417. The field of view for NICMOS2 is 19.″2 square, and the pixel scale is 0.″075. A 4 × 4 grid was observed in the F110W, F160W, F165M, and F207M filters, where each position in the grid was observed twice in each filter with a dither offset of ∼20 pixels in both right ascension and declination. The total integration time per position in the grid was 512 s for F110W, 352 s for F160W, 576 s for F165M, and 288 s for F207M. All the images were obtained in nondestructive readout mode with a total of 16 readouts in each exposure.

The full width at half-maxima of the point-spread function (PSF) are 0.″12, 0.″15, and 0.″20 for the F110W, F160W, and F207M bands, respectively. Table 1 contains the observing log.

The images were processed using a combination of IRAF scripts, C programs, and IDL scripts. The basic reduction was performed using the NICRED procedure (Lehár et al. 2000), which performs linearity corrections, cosmic-ray rejection, dark subtraction, and flat-fielding and determines photon rates. Synthetic darks were used based on the software NICRED. The pedestal effect was removed from each frame, also using NICRED. Bad pixels were identified and corrected using the IRAF task *fixpix*. Finally, for each filter, the images were registered and a mosaic was created using the average of the two dithered exposures at each position in the mosaic. A color composite of the observed region is shown in Figure 1, where F110W is blue, F160W is green, and F207M is red.

2.2. *Source Detection and Photometry*

Point sources in each of the mosaics were identified using the IRAF implementation of DAOFIND with a 5 σ detection threshold. False detections in the form of noise peaks or structures in the PSF were eliminated by comparing the source lists from each filter and a visual inspection of each source detected by DAOFIND. Since the location of features in the PSF for a given star is dependent on wavelength, the use of different filters helps in separating faint stars next to bright stars from structure in the bright-star PSF.

TABLE 1

Observing Log for the NICMOS2 Observations

Filter	Observation Date	Exposure Time (s)
F110W.....	1997 Dec 1	2 × 256
F160W.....	1997 Dec 1	2 × 176
F165M.....	1997 Dec 5	2 × 288
F207M.....	1997 Dec 5	2 × 144

Aperture photometry was performed using the APPHOT package in IRAF. An aperture of 3.5 pixel radius was used to measure the flux of the object, and the background was measured in an annulus from 10 to 15 pixels. For 10 objects an annulus of 2 pixels was used to measure the object flux because they were close to bright stars. The choice of a relatively large aperture for the majority of the sources was to limit photometric errors due to the variations in the PSF across the field of view of the NICMOS2 camera. Some 40 stars with no (or very little) nebulosity associated with them were used to determine aperture corrections for the photometry in each filter. The NICMOS2 photometry was measured relative to a 10 pixel radius aperture and is presented in the VEGAMAG system. The astrometry was done relative to Carpenter et al. (1997). Some 25 stars in common were used to fit a second-order polynomial in both right ascension and declination. The final rms was 0.″1. A comparison with the Two Micron All Sky Survey (2MASS) showed an offset by 0.″5 in right ascension and −0.″3 in declination relative to our astrometry. We corrected the astrometry for this offset, and the rms compared to 2MASS is then 0.″2 for eight relatively bright isolated sources. Table 2 presents the photometry and coordinates for the 181 sources detected, together with 2MASS IDs where available. Where more than one source was within 1″ in the *HST* NICMOS2 survey, we have chosen the brightest source in our observations as the 2MASS source. In four cases, two sources of roughly equal brightness in the NICMOS2 data were identified as one object by 2MASS. Both objects have been given the 2MASS ID and are marked with an asterisk.

The photometry has been converted into the CIT system using 41 stars in common with Carpenter et al. (1997). The stars covered a color range $0.4 \leq m_{\rm F160W} - m_{\rm F207M} \leq 3.2$, where $m_{\rm F160W}$ and $m_{\rm F207M}$ are the magnitudes in the F160W and F207M bands, respectively. Least-squares fits were performed to convert the NICMOS2 photometry to the CIT system, resulting in fits given by:

$$m_J = m_{\rm F110W} - (0.789 \pm 0.025) - (0.200 \pm 0.027)(m_{\rm F160W} - m_{\rm F207M}), \quad (1)$$

$$m_H = m_{\rm F160W} - (0.089 \pm 0.015) - (0.264 \pm 0.013)(m_{\rm F160W} - m_{\rm F207M}), \quad (2)$$

$$m_K = m_{\rm F207M} - (0.214 \pm 0.018) - (0.306 \pm 0.012)(m_{\rm F160M} - m_{\rm F207M}). \quad (3)$$

The photometry reaches roughly 2.5 mag deeper in the *J* band than the observations by Carpenter et al. (1997).

2.3. *Completeness Limits*

Artificial-star experiments have been performed in order to assess the completeness limits of the data. Synthetic PSFs have

FIG. 1.—*HST* NICMOS2 F110W (*blue*), F160W (*green*), and F207M (*red*) color composite of the central $1' \times 1'$ of Mon R2. The faintest (*red*) stars seen have a magnitude of $m_{\rm F207M} \sim 19.5$ mag. North is up and east left. The coordinates of the bright red source in the center of the image are (R.A., decl.) = ($06^{\rm h}07^{\rm m}45\overset{\rm s}{.}77$, $-06^\circ 22' 53\overset{''}{.}6$).

been created for each filter, using the Tiny Tim software (Krist et al. 1998), and a total of 160 artificial stars have been placed in each mosaic. The fraction of artificial stars recovered as a function of magnitude in each filter is presented in Table 3. All the recovery fractions are for a 5 σ threshold and were subject to visual inspection in a way identical to that used to detect sources in our survey. We have adopted the 90% completeness limit in this paper, which corresponds to the following limiting magnitudes: $m_{\rm F110W} = 21.5$, $m_{\rm F160W} = 20.5$, and $m_{\rm F207M} = 18.0$ mag.

3. RESULTS

We present the basic results from the photometry. Objects are placed in the H-R diagram in § 3.1 based on the effective temperature estimate derived through the flux ratio between F165M and F160W and the dereddened *J*-band magnitudes. In § 3.2 we discuss the $J - H$ versus *J* color-magnitude diagram and the $H - K$ versus $J - H$ color-color diagram. Throughout this section, we assume that all but two very blue bright stars are cluster members. The two blue stars have $J - H \leq 0.5$ mag and are assumed to be foreground objects. We have no direct estimate of the number of field stars expected toward Mon R2 that would contaminate our sample at the sensitivity of these observations. As an indirect test we have downloaded the 2MASS point sources located in a 2° region centered on $l = 214\overset{\circ}{.}3$, $b = -15\overset{\circ}{.}4$, where the coordinates for Mon R2 are $l = 213\overset{\circ}{.}7$, $b = -12\overset{\circ}{.}6$. The 2MASS *H*-band luminosity function is a power law down to the completeness limit of $H \sim 15$ mag. Assuming the field star population would follow a power law to faint magnitudes, we would expect ~45 field stars within our field of view down to $H = 20.5$ mag. However, the dust in the molecular cloud acts as a screen limiting the number of background stars we detect. Carpenter et al. (1997) found the average extinction from the molecular cloud to be $A_V = 50$ mag in the

TABLE 2

THE *HST* NICMOS2 PHOTOMETRY FOR MON R2

ID	R.A. (J2000.0)	Decl. (J2000.0)	F110W	F160W	F165M	F207M	2MASS ID
1.....	06 07 44.98	−06 23 25.8	23.11 ± 0.51	17.32 ± 0.05	17.10 ± 0.05	14.47 ± 0.06	06074492−0623257
2.....	06 07 45.63	−06 23 25.1	24.55 ± 1.21	19.77 ± 0.07	19.41 ± 0.07	17.07 ± 0.07	...
3.....	06 07 43.89	−06 23 26.8	18.58 ± 0.03	16.20 ± 0.04	15.90 ± 0.04	15.48 ± 0.06	...
4.....	06 07 44.82	−06 23 25.8	17.34 ± 0.03	14.77 ± 0.03	14.55 ± 0.03	13.89 ± 0.05	06074483−0623260
5.....	06 07 44.26	−06 23 25.5	16.12 ± 0.04	13.81 ± 0.04	13.58 ± 0.04	13.04 ± 0.06	06074426−0623256
6.....	06 07 47.67	−06 23 22.0	20.17 ± 0.04	18.45 ± 0.04	18.15 ± 0.04	17.90 ± 0.08	...
7.....	06 07 46.08	−06 23 21.8	18.62 ± 0.03	15.92 ± 0.03	15.68 ± 0.03	15.01 ± 0.05	...
8.....	06 07 44.98	−06 23 21.9	21.13 ± 0.05	17.56 ± 0.03	17.29 ± 0.03	16.17 ± 0.05	...
9.....	06 07 47.23	−06 23 18.8	20.88 ± 0.05	18.74 ± 0.04	18.51 ± 0.04	18.03 ± 0.08	...
10.....	06 07 44.53	−06 23 21.4	17.75 ± 0.04	14.96 ± 0.04	14.67 ± 0.04	13.63 ± 0.06	06074454−0623214
11.....	06 07 45.31	−06 23 20.2	15.51 ± 0.04	12.99 ± 0.04	12.76 ± 0.04	12.13 ± 0.06	06074531−0623202
12.....	06 07 43.82	−06 23 21.5	21.76 ± 0.11	18.46 ± 0.04	18.14 ± 0.04	17.08 ± 0.07	...
13.....	06 07 45.21	−06 23 19.5	18.62 ± 0.04	16.35 ± 0.04	16.06 ± 0.04	15.62 ± 0.07	...
14.....	06 07 46.64	−06 23 17.3	15.26 ± 0.04	12.80 ± 0.04	12.90 ± 0.04	12.09 ± 0.06	06074665−0623175
15.....	06 07 45.68	−06 23 17.7	18.91 ± 0.04	16.26 ± 0.04	16.02 ± 0.04	15.37 ± 0.07	...
16.....	06 07 43.96	−06 23 18.5	17.00 ± 0.04	14.52 ± 0.04	14.29 ± 0.04	13.71 ± 0.06	06074396−0623184
17.....	06 07 44.10	−06 23 18.2	21.25 ± 0.06	18.47 ± 0.04	18.28 ± 0.04	17.26 ± 0.07	...
18.....	06 07 45.49	−06 23 16.0	16.32 ± 0.04	14.06 ± 0.04	13.84 ± 0.04	13.43 ± 0.06	06074549−0623160
19.....	06 07 44.95	−06 23 16.4	22.56 ± 0.16	19.34 ± 0.05	19.06 ± 0.05	17.05 ± 0.05	...
20.....	06 07 46.31	−06 23 13.7	18.43 ± 0.04	16.00 ± 0.04	15.72 ± 0.04	15.21 ± 0.07	06074631−0623128
21.....	06 07 44.62	−06 23 15.3	22.75 ± 0.15	17.75 ± 0.04	17.42 ± 0.04	15.56 ± 0.06	...
22.....	06 07 45.65	−06 23 14.1	18.46 ± 0.04	16.29 ± 0.04	16.06 ± 0.04	15.71 ± 0.07	...
23.....	06 07 44.37	−06 23 15.4	...	20.90 ± 0.17	20.79 ± 0.18	18.54 ± 0.12	...
24.....	06 07 44.48	−06 23 15.2	...	20.43 ± 0.12	20.40 ± 0.14	17.49 ± 0.08	...
25.....	06 07 47.74	−06 23 11.8	16.98 ± 0.04	15.01 ± 0.04	14.77 ± 0.04	14.45 ± 0.06	...
26.....	06 07 47.12	−06 23 12.2	21.33 ± 0.07	18.75 ± 0.05	18.47 ± 0.05	17.74 ± 0.09	...
27.....	06 07 46.69	−06 23 12.6	15.84 ± 0.04	13.58 ± 0.04	13.35 ± 0.04	12.87 ± 0.06	06074669−0623125
28.....	06 07 44.80	−06 23 14.4	16.95 ± 0.03	13.79 ± 0.03	13.59 ± 0.03	12.59 ± 0.05	06074482−0623144
29.....	06 07 46.33	−06 23 12.1	20.55 ± 0.05	16.52 ± 0.04	16.21 ± 0.04	14.37 ± 0.06	...
30.....	06 07 45.46	−06 23 12.9	21.62 ± 0.14	18.59 ± 0.08	18.33 ± 0.08	17.50 ± 0.12	...
31.....	06 07 47.26	−06 23 10.5	24.16 ± 0.67	21.84 ± 0.69	22.11 ± 1.15	18.99 ± 0.24	...
32.....	06 07 43.95	−06 23 13.0	21.38 ± 0.07	16.62 ± 0.04	16.40 ± 0.04	14.10 ± 0.06	06074393−0623130
33.....	06 07 46.23	−06 23 10.4	...	...	...	17.91 ± 0.18	...
34.....	06 07 45.73	−06 23 10.9	20.83 ± 0.05	17.38 ± 0.03	17.06 ± 0.03	15.79 ± 0.05	06074579−0623113
35.....	06 07 45.11	−06 23 10.8	20.79 ± 0.06	16.52 ± 0.04	16.07 ± 0.04	14.16 ± 0.06	06074593−0623110
36.....	06 07 45.80	−06 23 09.6	20.79 ± 0.04	16.93 ± 0.02	16.63 ± 0.02	15.24 ± 0.04	06074500−0623113
37.....	06 07 45.96	−06 23 09.2	21.37 ± 0.14	17.80 ± 0.04	17.63 ± 0.04	15.67 ± 0.04	...
38.....	06 07 46.16	−06 23 09.0	...	19.18 ± 0.09	19.02 ± 0.09	16.35 ± 0.06	...
39.....	06 07 46.86	−06 23 07.9	16.73 ± 0.02	14.64 ± 0.02	14.39 ± 0.02	13.90 ± 0.03	06074686−0623076
40.....	06 07 43.99	−06 23 10.6	19.51 ± 0.03	16.63 ± 0.03	16.36 ± 0.03	15.60 ± 0.05	...
41.....	06 07 43.68	−06 23 10.4	17.50 ± 0.03	15.12 ± 0.03	14.84 ± 0.03	14.29 ± 0.05	06074370−0623107
42.....	06 07 45.16	−06 23 08.7	20.17 ± 0.04	16.42 ± 0.03	16.16 ± 0.03	14.96 ± 0.05	06074516−0623103
43.....	06 07 45.42	−06 23 08.2	19.23 ± 0.03	15.62 ± 0.03	15.11 ± 0.03	13.86 ± 0.05	06074542−0623092
44.....	06 07 44.81	−06 23 08.4	24.04 ± 0.68	19.33 ± 0.04	19.08 ± 0.03	16.69 ± 0.04	...
45.....	06 07 45.89	−06 23 07.3	22.60 ± 0.16	19.47 ± 0.04	19.21 ± 0.04	17.65 ± 0.05	...
46.....	06 07 46.64	−06 23 05.9	20.61 ± 0.12	17.02 ± 0.07	16.78 ± 0.07	15.41 ± 0.08	06074661−0623058
47.....	06 07 47.25	−06 23 05.1	21.95 ± 0.15	19.59 ± 0.08	19.27 ± 0.08	18.18 ± 0.15	...
48.....	06 07 46.62	−06 23 05.7	21.01 ± 0.19	18.23 ± 0.09	17.94 ± 0.09	16.45 ± 0.08	...
49.....	06 07 45.64	−06 23 06.5	20.92 ± 0.05	16.55 ± 0.03	16.23 ± 0.03	14.78 ± 0.05	...
50.....	06 07 47.84	−06 23 03.7	16.52 ± 0.03	13.82 ± 0.03	13.58 ± 0.03	12.82 ± 0.05	06074784−0623038
51.....	06 07 45.03	−06 23 06.5	20.49 ± 0.04	16.78 ± 0.03	16.68 ± 0.03	15.49 ± 0.05	06074503−0623060
52.....	06 07 45.08	−06 23 06.0	21.60 ± 0.11	17.03 ± 0.04	16.71 ± 0.04	15.18 ± 0.07	...
53.....	06 07 46.13	−06 23 04.5	17.19 ± 0.04	12.83 ± 0.04	12.57 ± 0.04	10.78 ± 0.06	06074615−0623046
54.....	06 07 44.62	−06 23 05.3	19.96 ± 0.04	16.66 ± 0.04	16.39 ± 0.04	15.25 ± 0.07	06074470−0623044
55.....	06 07 48.07	−06 23 01.9	23.92 ± 0.81	18.65 ± 0.04	18.34 ± 0.04	16.13 ± 0.05	06074807−0623017
56.....	06 07 44.80	−06 23 05.1	17.33 ± 0.04	15.51 ± 0.04	15.27 ± 0.04	15.19 ± 0.07	06074470−0623044
57.....	06 07 45.88	−06 23 03.5	22.96 ± 0.38	18.92 ± 0.04	18.56 ± 0.04	16.06 ± 0.05	...
58.....	06 07 47.67	−06 23 01.1	18.91 ± 0.04	16.95 ± 0.07	16.64 ± 0.07	16.56 ± 0.28	...
59.....	06 07 45.26	−06 23 03.2	22.02 ± 0.10	17.65 ± 0.04	17.58 ± 0.04	15.31 ± 0.06	...
60.....	06 07 44.62	−06 23 03.9	...	19.66 ± 0.14	19.21 ± 0.11	16.52 ± 0.08	...
61.....	06 07 46.22	−06 23 01.9	12.34 ± 0.04	11.57 ± 0.04	11.45 ± 0.04	11.63 ± 0.06	06074622−0623022
62.....	06 07 46.02	−06 23 01.6	...	18.52 ± 0.07	18.31 ± 0.06	14.78 ± 0.06	...
63.....	06 07 45.67	−06 23 01.9	23.57 ± 0.47	19.77 ± 0.09	19.48 ± 0.09	17.01 ± 0.08	...
64.....	06 07 45.85	−06 23 01.4	25.11 ± 3.73	21.61 ± 0.29	20.85 ± 0.18	18.57 ± 0.13	...
65.....	06 07 45.99	−06 23 01.1	21.89 ± 0.17	20.78 ± 0.19	20.26 ± 0.17	18.08 ± 0.11	...
66.....	06 07 45.04	−06 23 01.8	21.59 ± 0.18	18.76 ± 0.11	18.43 ± 0.09	17.49 ± 0.13	06074495−0623010

TABLE 2—*Continued*

ID	R.A. (J2000.0)	Decl. (J2000.0)	F110W	F160W	F165M	F207M	2MASS ID
67.....	06 07 46.16	−06 23 00.4	22.44 ± 0.38	18.79 ± 0.07	18.41 ± 0.06	16.12 ± 0.07	...
68.....	06 07 45.65	−06 23 00.8	26.05 ± 3.84	21.88 ± 0.56	21.53 ± 0.46	18.51 ± 0.17	...
69.....	06 07 46.01	−06 23 00.3	23.67 ± 1.21	...	23.56 ± 4.82	21.81 ± 3.48	...
70.....	06 07 45.98	−06 22 59.9	23.32 ± 0.82	...	...	19.46 ± 0.46	...
71.....	06 07 45.71	−06 23 00.0	22.59 ± 0.22	18.03 ± 0.03	17.69 ± 0.03	15.05 ± 0.05	...
72.....	06 07 45.64	−06 22 59.4	23.07 ± 0.23	21.15 ± 0.29	20.38 ± 0.16	19.48 ± 0.43	...
73.....	06 07 46.75	−06 22 57.6	21.64 ± 0.17	18.45 ± 0.10	18.07 ± 0.10	16.49 ± 0.10	...
74.....	06 07 46.72	−06 22 57.5	20.21 ± 0.08	16.54 ± 0.07	16.19 ± 0.07	14.95 ± 0.07	06074674−0622562
75.....	06 07 47.53	−06 22 56.5	17.33 ± 0.04	15.11 ± 0.04	14.84 ± 0.04	14.35 ± 0.07	...
76.....	06 07 46.89	−06 22 57.0	20.58 ± 0.06	18.54 ± 0.04	18.25 ± 0.04	17.72 ± 0.08	...
77.....	06 07 47.84	−06 22 56.1	14.23 ± 0.04	10.43 ± 0.04	10.16 ± 0.04	8.21 ± 0.06	06074786−0622559
78.....	06 07 47.74	−06 22 56.1	17.89 ± 0.05	14.75 ± 0.04	14.45 ± 0.04	13.04 ± 0.06	...
79.....	06 07 46.28	−06 22 57.1	...	18.05 ± 0.04	18.22 ± 0.05	15.31 ± 0.06	...
80.....	06 07 47.89	−06 22 55.2	15.25 ± 0.04	11.91 ± 0.04	11.68 ± 0.04	9.73 ± 0.06	...
81.....	06 07 46.43	−06 22 56.3	22.72 ± 0.25	19.58 ± 0.07	19.19 ± 0.06	17.69 ± 0.08	...
82.....	06 07 47.68	−06 22 55.0	15.70 ± 0.04	13.66 ± 0.04	13.34 ± 0.04	12.78 ± 0.06	...
83.....	06 07 46.89	−06 22 55.6	19.27 ± 0.04	18.27 ± 0.04	18.07 ± 0.04	18.15 ± 0.08	...
84.....	06 07 45.02	−06 22 56.9	22.39 ± 0.12	18.05 ± 0.05	17.76 ± 0.05	16.14 ± 0.07	06074488−0622563
85.....	06 07 47.89	−06 22 54.0	17.08 ± 0.04	13.85 ± 0.04	13.71 ± 0.04	12.42 ± 0.08	...
86.....	06 07 46.69	−06 22 54.8	19.66 ± 0.05	15.88 ± 0.04	15.61 ± 0.04	14.42 ± 0.06	...
87.....	06 07 47.38	−06 22 53.9	17.61 ± 0.04	15.05 ± 0.04	14.81 ± 0.04	14.03 ± 0.06	...
88.....	06 07 45.45	−06 22 55.7	23.27 ± 0.34	19.46 ± 0.09	19.08 ± 0.08	17.65 ± 0.11	...
89.....	06 07 45.72	−06 22 55.0	23.12 ± 0.30	18.90 ± 0.04	18.62 ± 0.04	15.44 ± 0.05	...
90.....	06 07 47.67	−06 22 53.0	20.85 ± 0.08	18.02 ± 0.10	17.74 ± 0.10	16.04 ± 0.09	...
91.....	06 07 46.03	−06 22 54.5	25.26 ± 2.81	19.39 ± 0.09	19.00 ± 0.08	16.60 ± 0.07	...
92.....	06 07 46.37	−06 22 54.0	22.33 ± 0.20	19.59 ± 0.09	19.24 ± 0.08	17.83 ± 0.09	...
93.....	06 07 46.10	−06 22 54.1	...	18.57 ± 0.04	18.40 ± 0.04	15.39 ± 0.05	...
94.....	06 07 45.64	−06 22 54.3	24.30 ± 0.67	18.46 ± 0.04	18.30 ± 0.04	15.97 ± 0.05	...
95.....	06 07 44.14	−06 22 55.5	23.41 ± 0.29	20.73 ± 0.17	20.32 ± 0.15	19.14 ± 0.24	...
96.....	06 07 45.80	−06 22 53.3	19.54 ± 0.02	14.59 ± 0.02	14.52 ± 0.02	9.77 ± 0.03	...
97.....	06 07 46.01	−06 22 53.0	23.28 ± 0.36	19.93 ± 0.09	19.75 ± 0.08	16.99 ± 0.06	...
98.....	06 07 46.60	−06 22 52.4	19.67 ± 0.03	16.12 ± 0.03	15.77 ± 0.03	14.69 ± 0.05	...
99.....	06 07 45.69	−06 22 52.4	22.92 ± 0.31	18.80 ± 0.04	18.87 ± 0.04	15.42 ± 0.04	...
100.....	06 07 45.75	−06 22 51.7	22.53 ± 0.19	20.97 ± 0.19	21.18 ± 0.34	16.68 ± 0.07	...
101.....	06 07 46.42	−06 22 50.8	22.43 ± 0.14	19.91 ± 0.13	19.75 ± 0.13	18.33 ± 0.19	...
102.....	06 07 44.54	−06 22 52.6	23.87 ± 0.60	20.54 ± 0.13	20.20 ± 0.12	17.76 ± 0.06	06074443−0622523
103.....	06 07 46.47	−06 22 50.4	21.84 ± 0.08	17.90 ± 0.03	17.60 ± 0.03	16.03 ± 0.05	...
104.....	06 07 43.64	−06 22 52.5	16.40 ± 0.04	13.84 ± 0.04	13.64 ± 0.04	12.80 ± 0.06	06074361−0622519*
105.....	06 07 46.38	−06 22 49.5	21.53 ± 0.08	18.22 ± 0.04	17.83 ± 0.04	16.50 ± 0.06	...
106.....	06 07 46.18	−06 22 49.6	23.01 ± 0.24	19.87 ± 0.16	19.50 ± 0.14	17.52 ± 0.16	...
107.....	06 07 45.60	−06 22 50.1	21.99 ± 0.10	17.74 ± 0.03	17.48 ± 0.03	15.70 ± 0.05	...
108.....	06 07 46.26	−06 22 49.4	23.11 ± 0.28	17.94 ± 0.05	17.61 ± 0.05	15.46 ± 0.07	...
109.....	06 07 45.70	−06 22 49.4	21.68 ± 0.09	17.13 ± 0.03	16.79 ± 0.03	15.11 ± 0.05	...
110.....	06 07 44.10	−06 22 50.9	22.68 ± 0.25	19.63 ± 0.07	19.25 ± 0.06	18.04 ± 0.09	...
111.....	06 07 43.60	−06 22 51.3	15.61 ± 0.04	13.15 ± 0.04	12.93 ± 0.04	12.43 ± 0.06	06074361−0622519*
112.....	06 07 45.56	−06 22 49.3	22.61 ± 0.19	17.51 ± 0.04	17.19 ± 0.04	14.94 ± 0.07	...
113.....	06 07 46.33	−06 22 46.8	20.40 ± 0.05	17.12 ± 0.04	16.78 ± 0.04	15.87 ± 0.07	06074636−0622467
114.....	06 07 45.30	−06 22 47.1	22.72 ± 0.20	18.70 ± 0.06	18.41 ± 0.05	16.19 ± 0.07	...
115.....	06 07 46.27	−06 22 45.6	21.50 ± 0.11	17.99 ± 0.06	17.72 ± 0.05	16.40 ± 0.08	...
116.....	06 07 46.49	−06 22 45.0	22.63 ± 0.17	17.62 ± 0.04	17.41 ± 0.04	15.09 ± 0.07	...
117.....	06 07 45.07	−06 22 46.3	20.86 ± 0.06	16.71 ± 0.04	16.48 ± 0.04	14.87 ± 0.06	...
118.....	06 07 44.97	−06 22 46.4	21.44 ± 0.08	17.52 ± 0.04	17.23 ± 0.04	15.92 ± 0.07	...
119.....	06 07 45.16	−06 22 45.7	22.76 ± 0.23	20.80 ± 0.16	20.37 ± 0.13	19.45 ± 0.34	...
120.....	06 07 43.74	−06 22 46.7	16.92 ± 0.09	14.71 ± 0.09	14.40 ± 0.09	14.00 ± 0.10	06074374−0622467
121.....	06 07 43.75	−06 22 46.4	17.77 ± 0.09	15.41 ± 0.09	15.15 ± 0.09	14.70 ± 0.10	...
122.....	06 07 44.45	−06 22 44.8	22.07 ± 0.13	17.42 ± 0.04	17.14 ± 0.04	15.49 ± 0.06	...
123.....	06 07 46.40	−06 22 42.7	17.74 ± 0.04	15.21 ± 0.04	15.00 ± 0.04	14.42 ± 0.06	06074640−0622432
124.....	06 07 43.55	−06 22 44.6	19.28 ± 0.09	16.04 ± 0.09	15.74 ± 0.09	14.58 ± 0.10	06074356−0622448*
125.....	06 07 43.56	−06 22 44.6	18.74 ± 0.09	15.46 ± 0.09	15.17 ± 0.09	14.20 ± 0.10	06074356−0622448*
126.....	06 07 43.90	−06 22 44.2	22.41 ± 0.20	20.15 ± 0.07	19.84 ± 0.07	18.93 ± 0.12	...
127.....	06 07 46.94	−06 22 40.9	21.87 ± 0.09	17.79 ± 0.03	17.49 ± 0.03	16.10 ± 0.05	...
128.....	06 07 46.27	−06 22 41.0	23.00 ± 0.27	20.57 ± 0.20	20.00 ± 0.16	18.91 ± 0.33	...
129.....	06 07 44.99	−06 22 42.2	24.44 ± 1.09	19.35 ± 0.07	18.97 ± 0.06	17.48 ± 0.08	...
130.....	06 07 45.81	−06 22 41.4	24.99 ± 1.97	19.06 ± 0.05	18.88 ± 0.05	16.53 ± 0.05	...
131.....	06 07 44.76	−06 22 41.5	24.28 ± 0.96	20.88 ± 0.12	20.82 ± 0.13	18.33 ± 0.08	...
132.....	06 07 47.43	−06 22 38.5	24.01 ± 0.44	23.40 ± 1.12	24.70 ± 4.58	18.28 ± 0.09	...
133.....	06 07 44.48	−06 22 41.2	18.30 ± 0.04	15.11 ± 0.04	14.88 ± 0.04	13.93 ± 0.06	06074449−0622414

TABLE 2—*Continued*

ID	R.A. (J2000.0)	Decl. (J2000.0)	F110W	F160W	F165M	F207M	2MASS ID
134.....	06 07 46.36	−06 22 38.8	21.17 ± 0.07	17.37 ± 0.04	17.03 ± 0.04	15.79 ± 0.07	...
135.....	06 07 44.96	−06 22 40.0	16.57 ± 0.03	13.86 ± 0.03	13.90 ± 0.03	13.02 ± 0.05	06074496−0622401
136.....	06 07 46.32	−06 22 38.4	18.28 ± 0.02	15.13 ± 0.02	14.82 ± 0.02	13.43 ± 0.03	...
137.....	06 07 46.59	−06 22 37.2	22.06 ± 0.12	19.68 ± 0.10	19.47 ± 0.11	18.05 ± 0.12	...
138.....	06 07 43.70	−06 22 40.1	20.22 ± 0.04	15.90 ± 0.03	15.65 ± 0.03	13.46 ± 0.05	06074371−0622402
139.....	06 07 45.78	−06 22 37.6	17.95 ± 0.03	15.52 ± 0.03	15.06 ± 0.03	14.51 ± 0.05	...
140.....	06 07 43.65	−06 22 37.7	22.41 ± 0.11	19.36 ± 0.05	19.13 ± 0.05	17.40 ± 0.07	...
141.....	06 07 46.58	−06 22 36.8	22.16 ± 0.14	20.05 ± 0.08	19.76 ± 0.08	18.40 ± 0.08	06074658−0622370
142.....	06 07 45.60	−06 22 37.4	17.58 ± 0.03	13.26 ± 0.03	13.04 ± 0.03	11.03 ± 0.05	06074563−0622380
143.....	06 07 47.01	−06 22 35.4	19.83 ± 0.03	16.74 ± 0.03	16.42 ± 0.03	15.62 ± 0.05	...
144.....	06 07 43.84	−06 22 38.4	22.91 ± 0.22	19.27 ± 0.03	18.79 ± 0.03	17.01 ± 0.05	...
145.....	06 07 47.48	−06 22 34.4	22.98 ± 0.17	20.56 ± 0.08	20.13 ± 0.06	19.66 ± 0.25	...
146.....	06 07 45.74	−06 22 35.3	22.73 ± 0.18	18.24 ± 0.02	18.03 ± 0.02	15.56 ± 0.03	06074565−0622355
147.....	06 07 43.55	−06 22 37.0	18.23 ± 0.04	15.47 ± 0.04	15.11 ± 0.04	14.51 ± 0.06	06074355−0622371
148.....	06 07 46.60	−06 22 33.5	16.28 ± 0.04	13.56 ± 0.04	13.41 ± 0.04	12.45 ± 0.06	06074660−0622335
149.....	06 07 46.60	−06 22 33.0	...	15.54 ± 0.04	15.92 ± 0.04	14.35 ± 0.06	...
150.....	06 07 47.33	−06 22 32.0	...	22.20 ± 0.44	21.99 ± 0.43	21.74 ± 1.74	...
151.....	06 07 45.34	−06 22 33.8	20.43 ± 0.05	17.22 ± 0.04	16.85 ± 0.04	15.55 ± 0.07	06074540−0622334
152.....	06 07 45.44	−06 22 33.5	22.04 ± 0.10	17.31 ± 0.04	17.31 ± 0.04	14.63 ± 0.06	...
153.....	06 07 44.11	−06 22 34.5	24.27 ± 0.75	21.32 ± 0.17	21.16 ± 0.19	18.91 ± 0.11	...
154.....	06 07 45.94	−06 22 32.4	18.86 ± 0.04	15.33 ± 0.04	15.03 ± 0.04	13.77 ± 0.06	...
155.....	06 07 47.17	−06 22 31.2	16.25 ± 0.04	13.70 ± 0.04	13.50 ± 0.04	12.62 ± 0.06	06074717−0622313
156.....	06 07 44.52	−06 22 33.6	...	24.08 ± 2.36	25.67 ±1 2.71	19.13 ± 0.16	...
157.....	06 07 46.13	−06 22 29.2	24.96 ± 1.64	22.35 ± 0.59	21.56 ± 0.31	20.36 ± 0.41	...
158.....	06 07 44.24	−06 22 30.5	16.57 ± 0.09	14.64 ± 0.09	14.45 ± 0.09	14.19 ± 0.10	06074426−0622305*
159.....	06 07 44.26	−06 22 30.3	15.91 ± 0.09	14.05 ± 0.09	13.83 ± 0.09	13.63 ± 0.10	06074426−0622305*
160.....	06 07 47.35	−06 22 27.2	18.33 ± 0.04	16.67 ± 0.04	16.43 ± 0.04	16.25 ± 0.07	...
161.....	06 07 43.99	−06 22 30.0	17.17 ± 0.04	14.53 ± 0.04	14.25 ± 0.04	13.62 ± 0.06	06074398−0622301
162.....	06 07 43.82	−06 22 30.0	18.34 ± 0.04	15.83 ± 0.04	15.54 ± 0.04	14.89 ± 0.06	...
163.....	06 07 44.82	−06 22 28.9	21.04 ± 0.05	17.47 ± 0.03	17.31 ± 0.03	16.07 ± 0.05	06074485−0622300
164.....	06 07 45.33	−06 22 28.0	15.81 ± 0.04	14.02 ± 0.04	13.83 ± 0.04	13.63 ± 0.06	06074533−0622282
165.....	06 07 46.03	−06 22 25.5	16.44 ± 0.04	13.94 ± 0.04	13.62 ± 0.04	12.93 ± 0.06	06074602−0622242*
166.....	06 07 46.40	−06 22 24.4	17.79 ± 0.04	14.75 ± 0.04	14.51 ± 0.04	13.60 ± 0.06	06074641−0622245
167.....	06 07 45.65	−06 22 25.1	23.09 ± 0.29	21.22 ± 0.30	21.07 ± 0.23	18.81 ± 0.17	...
168.....	06 07 47.10	−06 22 23.4	25.87 ± 3.04	...	22.14 ± 0.43	19.19 ± 0.15	...
169.....	06 07 46.02	−06 22 23.7	15.82 ± 0.04	13.15 ± 0.04	12.84 ± 0.04	12.07 ± 0.06	06074602−0622242*
170.....	06 07 46.29	−06 22 23.2	21.42 ± 0.07	17.86 ± 0.04	17.55 ± 0.04	16.39 ± 0.07	...
171.....	06 07 45.70	−06 22 23.3	17.47 ± 0.03	15.50 ± 0.03	15.23 ± 0.03	14.96 ± 0.05	06074570−0622235
172.....	06 07 47.01	−06 22 20.7	17.81 ± 0.04	15.18 ± 0.04	14.94 ± 0.04	14.33 ± 0.06	06074702−0622208
173.....	06 07 46.31	−06 22 20.5	21.90 ± 0.15	19.27 ± 0.09	18.98 ± 0.08	17.39 ± 0.10	...
174.....	06 07 45.77	−06 22 20.5	18.42 ± 0.03	15.79 ± 0.03	15.50 ± 0.03	14.79 ± 0.05	...
175.....	06 07 44.14	−06 22 22.1	...	21.88 ± 0.28	20.65 ± 0.12	19.21 ± 0.14	...
176.....	06 07 45.18	−06 22 20.9	21.93 ± 0.12	19.29 ± 0.05	19.18 ± 0.05	18.92 ± 0.14	...
177.....	06 07 46.62	−06 22 19.4	23.10 ± 0.33	20.45 ± 0.18	20.31 ± 0.19	18.09 ± 0.10	...
178.....	06 07 47.52	−06 22 18.3	19.78 ± 0.04	16.11 ± 0.04	15.79 ± 0.04	14.04 ± 0.06	06074753−0622184
179.....	06 07 44.76	−06 22 20.8	22.27 ± 0.12	17.41 ± 0.03	17.12 ± 0.03	15.39 ± 0.05	...
180.....	06 07 46.41	−06 22 18.8	23.79 ± 0.76	18.48 ± 0.05	18.27 ± 0.05	16.28 ± 0.07	...
181.....	06 07 46.57	−06 22 18.5	17.77 ± 0.04	15.12 ± 0.04	14.83 ± 0.04	14.14 ± 0.06	06074656−0622188

NOTES.—Units of right ascension are hours, minutes, and seconds, and units of declination are degrees, arcminutes, and arcseconds. Asterisks indicate situations in this study in which two stars were identified as one object in 2MASS. Table 2 is also available in machine-readable form in the electronic edition of the *Astronomical Journal*.

central 45″ region and $A_V = 33$ mag, on average, across the central 3′ square region. If the field star luminosity function extrapolated from 2MASS is reddened by $A_V = 30$ mag, the surface density of field stars down to a limiting magnitude of $H = 20.5$ mag is expected to be one to two objects per square arcminute. We have also estimated the field star contamination using the synthetic Galactic model by Robin et al. (2003). The molecular cloud has been placed at 830 pc and assumed to extinct background sources by $A_V = 30$ mag. The model predicts that we should observe 10,464 sources per square degree down to $H = 20.5$ mag, where 6022 sources are predicted to be foreground sources. Thus, the model predicts 1.7 foreground objects and 1.2 background objects; the former is consistent with our identification of two blue foreground objects, and the latter is in agreement with the extrapolation from the 2MASS data.

3.1. *Effective Temperatures and Luminosities for Objects in Mon R2*

A water vapor absorption feature is present in the H band in the spectra of stars and brown dwarfs with temperatures at or below 4000 K (see, e.g., Allard et al. 2000). This feature is covered by the F160W filter and, since the F165M filter measures the continuum, the color $m_{\rm F165M} - m_{\rm F160W}$ for an object cooler than ~4000 K can be used to estimate the effective temperature. We

TABLE 3
FRACTION OF RECOVERED ARTIFICIAL STARS AS A FUNCTION OF MAGNITUDE FOR EACH FILTER

Magnitude	F110W (%)	F160W (%)	F165M (%)	F207M (%)
17.0	...	...	...	97
17.5	...	...	...	97
18.0	...	...	...	96
18.5	...	...	...	77
19.0	...	...	...	9
19.5	...	98	96	1
20.0	99	98	98	...
20.5	99	94	97	...
21.0	97	44	51	...
21.5	87	5	2	...
22.0	66	2	1	...
22.5	10	...	...	...
23.0	2	...	...	...

NOTE.—The detection limit was set to 5 σ.

have compared the $m_{F165M} - m_{F160W}$ colors, with the synthetic colors predicted by the atmosphere models of Hauschildt et al. (1999) and Allard et al. (2000) for objects above and below 2500 K, respectively. The $m_{F165M} - m_{F160W}$ versus $m_{F110W} - m_{F160W}$ color-color diagram is shown in Figure 2.

The reddening vector is parallel to the models for temperatures above ~3800 K ($m_{F165M} - m_{F160W} > -0.1$ mag), and no reliable temperature can be derived. There is a plateau from ~3800 to ~2700 K (spectral types M0 to M7.5), where a unique temperature can be obtained by projecting an observed point along the reddening vector until it intersects the temperature locus. The reddening vector crosses the models at two places for lower temperatures, and a unique temperature cannot be obtained. We have estimated the effective temperature for the sources located between ~3300 and ~2700 K that have magnitude errors smaller than 0.06 mag. An uncertainty of 0.06 mag translates into an uncertainty of the temperature determined from the model of ~10% for this temperature range. We have adopted the models with a surface gravity of $\log g = 4$, consistent with typical values of low-mass pre-main-sequence objects. We do not necessarily trust the magnitude of the extinction needed for the observations to intersect the temperature locus, due to uncertainties in the pseudocontinua predicted by the models. Previous studies have shown that the strength of the water bands in the *J* and *K* bands only depends weakly on the surface gravity (Wilking et al. 2004; Gorlova et al. 2003). It could thus be expected that the *H*-band water vapor absorption feature is also weakly dependent on gravity. Indeed, adopting a model with $\log g = 4.5$ only decreases the derived temperature by $\leq$50 K. Decreasing the surface gravity to $\log g = 3.5$ has a more complicated effect. Whereas the low-temperature regime ($\leq$3000 K) is unaffected, we would underestimate the temperature by ~300 K by incorrectly adopting the $\log g = 4.0$ model for objects with temperatures between 3000 and 3500 K. Leggett et al. (1996) compared the NextGen models to observed spectra of late-type stars. They found the predicted water bands to be deeper than observed for a given spectral type. The effect is that the models will predict a slightly too high temperature for a given water band strength. Najita et al. (2000) and Gorlova et al. (2003) find reasonable agreement between temperatures derived from comparison of water vapor indices from the models and spectral types. However, Luhman et al. (2003) found a systematic shift of spectral types relative to Najita et al. (2000) of one to two subtypes, which they attributed to the difference in the surface gravity between field dwarfs used to calibrate the index of pre-main-sequence objects. Based on the model prediction of the temperature accuracy and the indirect evidence from other water bands, we estimate our systematic uncertainties to be ±300 K for temperatures derived using the water vapor index.

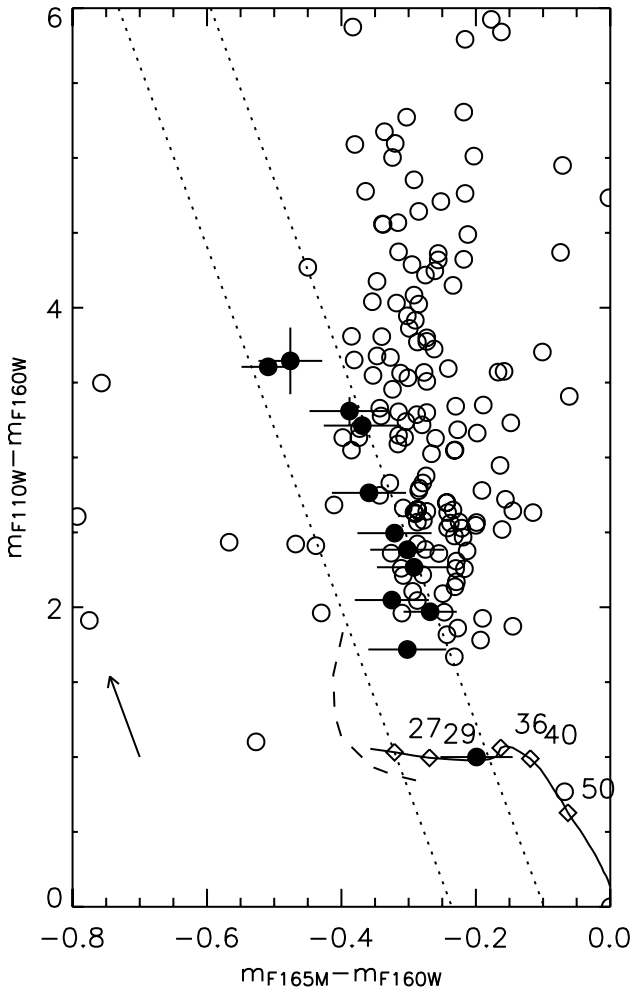

FIG. 2.—The $m_{F165M} - m_{F160W}$ vs. $m_{F110W} - m_{F160W}$ color-color diagram. Overplotted are the DUSTY models by Allard et al. (2000) for temperatures below 2500 K (*dashed line*) and the NextGen models by Hauschildt et al. (1999) for temperatures above 2500 K (*solid line*). The arrow indicates the magnitude and slope of $A_V = 5$ mag. The dotted lines indicate the region of the color-color diagram where a reliable temperature can be obtained if the photometric error in $m_{F165M} - m_{F160W}$ is less than ~0.06 mag. Objects for which the effective temperature has been derived are shown as filled circles, and the error bars are indicated for these objects. The effective temperatures at positions on the two models are shown in units of 100 K and marked on the model with diamonds.

Objects with a derived effective temperature in the range 2700–3300 K and with a photometric error $m_{F165M} - m_{F160W} <$ 0.06 mag are marked with filled circles in Figure 2. We determined the bolometric luminosity adopting formula (2) from Gorlova et al. (2003), which assumes $M_{bol} = 4.64$ and $BC_{V\odot} = -0.19$. The dominant source of error in the bolometric luminosity stems from uncertainties in the derived extinction. An error per filter of 0.06 mag will translate into an error in the visual extinction of $A_V \sim 0.75$ mag. Taking into account an error of ~10% in the bolometric correction and the distance uncertainty, we estimate the error in the logarithm of the bolometric luminosity to be 0.2. The objects are then placed in the H-R diagram, which is shown in Figure 3. We have not plotted source 83 in the H-R diagram.

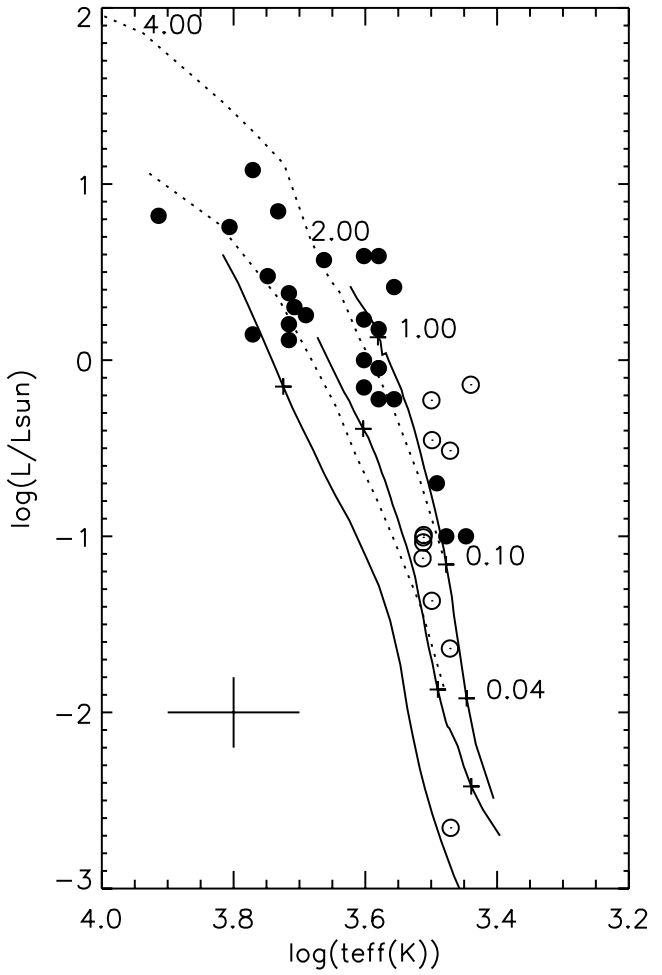

FIG. 3.—H-R diagram based on objects for which the effective temperature and luminosity have been derived in this study using the $m_{F165M} - m_{F160W}$ color (*open circles*) and objects from Carpenter et al. (1997; *filled circles*). Overplotted are the 1, 10, and 1000 Myr isochrones made from Baraffe et al. (1998; *solid lines*) and both Palla & Stahler (1999) 1 and 10 Myr isochrones (*dashed lines*). Plus signs mark 1, 0.1, and 0.04 $M_\odot$ on the Baraffe et al. isochrones. The Palla & Stahler (1999) isochrone covers the mass range 0.1–7 $M_\odot$. A typical error bar is shown.

Source 83 is a probable foreground source due to its very low extinction. Source 6 also appears underluminous. One possible reason for the underluminosity may be that the extinction has been underestimated due to unresolved scattered light (e.g., Wilking et al. 2004).

The objects from Carpenter et al. (1997) with effective temperature and luminosity estimates are shown in Figure 3 as well. The 1, 10, and 1000 Myr Baraffe et al. (1998) isochrones are shown. Since the Baraffe et al. (1998) models only extend to 1.4 $M_\odot$, we have overplotted 1 and 10 Myr Palla & Stahler (1999) isochrones to cover masses up to 7 $M_\odot$. Table 4 summarizes the parameters for the sources with the effective temperature derived from the water band method described above.

Although a large fraction of the objects below 1 $M_\odot$ are located close to the 1 Myr isochrone, there appears to be a large scatter. Some of the scatter is due to errors in the estimates of the effective temperatures and luminosities, and some of the scatter might be real. However, most of the objects that appear to be older than 1 Myr are more massive than 1 $M_\odot$, which is the maximum mass we attempt to constrain the IMF. We find that for the objects in the H-R diagram with masses between 0.04 and 0.4 $M_\odot$, seven objects are 1 Myr or younger and six are older than 1 Myr. A median age of 1 Myr appears to be appropriate for the lower mass content in Mon R2.

TABLE 4

PHYSICAL PARAMETERS FOR SOURCES FOR WHICH WE HAVE ESTIMATED EFFECTIVE TEMPERATURE

ID	A_V[a]	T_{eff}	M_J	Excess[b]	log L
3.....	10.4	3250	5.29	N	−1.00
6.....	1.4	2950	9.35	Y	−2.66
13.....	9.4	3250	5.59	N	−1.12
43.....	21.1	2750	2.93	Y	−0.14
82.....	4.6	2950	4.00	Y	−0.51
83.....	0.0	3150	10.54	Y	−3.11
105.....	17.7	3150	6.18	Y	−1.37
144.....	20.4	2950	6.81	Y	−1.64
147.....	14.2	3150	3.90	N	−0.45
151.....	16.7	3250	5.37	Y	−1.03
165.....	9.7	3150	3.33	Y	−0.28
171.....	6.5	3250	5.26	N	−1.00

[a] Derived from the color-magnitude and color-color diagrams in Figs. 4 and 5, as described in § 3.2.

[b] Estimated from the color-color diagram in Fig. 5.

3.2. *Color-Magnitude and Color-Color Diagrams*

We present in Figure 4 the $J - H$ versus J color-magnitude diagram for the inner 1′ square of Mon R2. Also shown are a

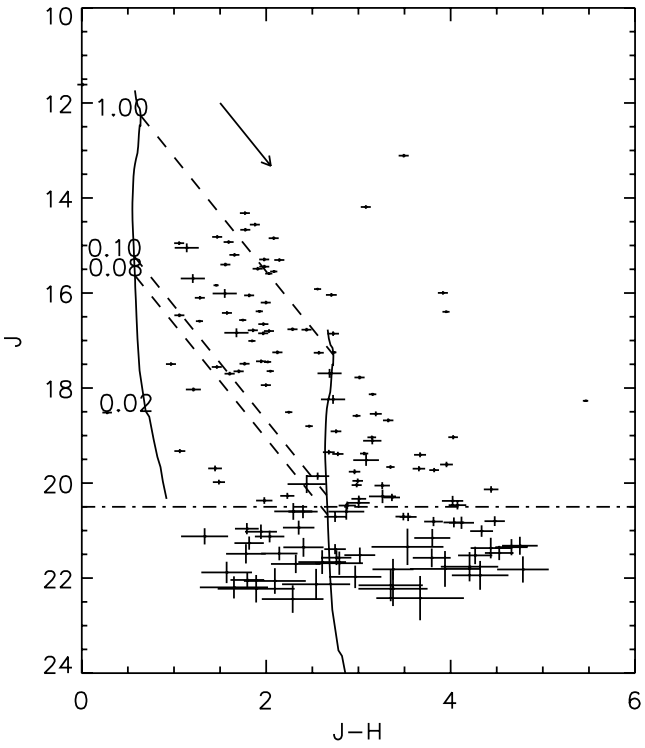

FIG. 4.—$J - H$ vs. J color-magnitude diagram for Mon R2 based on data from Table 2 converted into the CIT system. Overplotted as the solid lines are a 1 Myr isochrone from the Baraffe et al. (1998) models as discussed in the text and the same isochrone reddened by $A_V = 19$ mag. The symbol sizes indicate photometric error, where the error in the transformation into the CIT system has been included. The horizontal line indicates the 90% completeness limit of the observations. The arrow illustrates the effect of $A_V = 5$ mag extinction. Dashed lines are drawn between the unreddened and reddened isochrones at object masses of 1, 0.1, and 0.08 $M_\odot$. The location of an unreddened 0.02 $M_\odot$ object is marked.

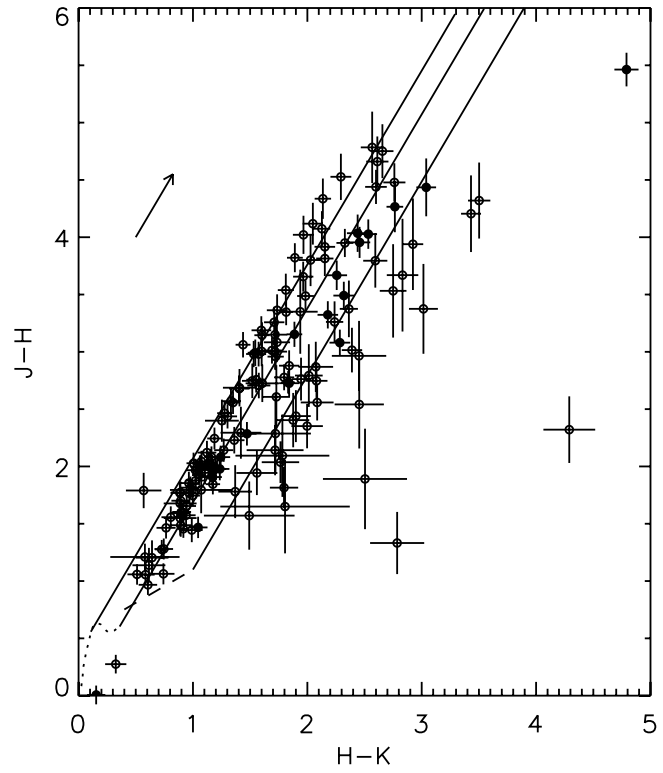

FIG. 5.—$H-K$ vs. $J-H$ color-color diagram for Mon R2 based on data in Table 2 converted into the CIT system. The open circles indicate stars not identified with any near-infrared excess, whereas the filled circles indicate stars with near-infrared excess and an estimated spectral type earlier than M6 (see text). The colors from Bessell & Brett (1988) for main-sequence stars with spectral types B8 to M6 are shown by the dotted line. The length of the arrow illustrates the effect of $A_V = 5$ mag extinction. The dashed line shows the unreddened T Tauri locus from Meyer et al. (1997). Extended from the main-sequence colors and the classical T Tauri slope are solid lines parallel to the reddening vector.

1 Myr isochrone created from the Baraffe et al. (1998) models, both unreddened and reddened by $A_V = 19$ mag and shifted with a distance modulus of 9.6 mag (830 pc). The Baraffe et al. models with $L_{\rm mix} = H_P$ are chosen, since they cover the whole mass range in which we attempt to constrain the IMF (0.02–1.0 $M_\odot$) and they are tied to the atmosphere models used in § 3.1.

In order to convert the effective temperatures and bolometric magnitudes provided by the models to observables, we have used the main-sequence colors from Bessell & Brett (1988) and the temperature scales from Schmidt-Kaler (1982) and Bessell (1991) for objects earlier and later than spectral type K7, respectively. Data from Dahn et al. (2002) have been used for spectral types later than M6. The bolometric corrections and colors were interpolated using spline interpolation. Due to large scatter observed in the intrinsic colors and magnitudes for the late-type objects, a linear fit has been performed for objects later than M6.

We expect the observed color of pre-main-sequence objects to be due to several effects. One is the intrinsic color of the object that depends on mass and age, which in turn fix $T_{\rm eff}$ and $\log g$. Another is the general interstellar extinction toward the object and the possible presence of a circumstellar disk associated with the object. From the color-magnitude diagram it is not possible to distinguish between the two latter effects. However, they can, at least partly, be separated in the $H-K$ versus $J-H$ color-color diagram. Objects without strong emission from a disk have colors resembling reddened main-sequence stars and therefore populate a confined region in the color-color diagram. Figure 5 shows the color-color diagram for Mon R2 in the CIT system. Overplotted are the colors for main-sequence stars from Bessell & Brett (1988), reddening vectors from stars with spectral type M6 and K7, and the dereddened classical T Tauri locus derived by Meyer et al. (1997). Objects with an excess have a larger reddening in $H-K$ relative to what would be expected from their $J-H$ color and are located to the right of the main-sequence stars in the color-color diagram.

A large fraction of the stars fall in the region expected for stars with no infrared excess and spectral type earlier than M6. The objects having larger than expected $H-K$ relative to the reddening vector extending from the M6 main-sequence star can be either stars with a spectral type earlier than M6 with an infrared excess or objects of later spectral type with or without infrared excess. The intrinsic colors for very late type objects (later than M6) almost overlap in the color-color diagram with the dereddened classical T Tauri locus. Thus, we cannot tell whether late spectral type objects have a disk from the color-color diagram alone.

The error adopted in $J-H$ by not being able to distinguish between an excess object and a late-type object is $\leq$0.1 mag, corresponding to $A_V \leq 1$ mag. We have therefore dereddened all objects in this part of the diagram to the T Tauri locus in order to establish the intrinsic magnitudes of the objects. For stars with colors consistent with main-sequence stars, they can in general be dereddened to two different intersections with the main-sequence colors. Therefore, we have dereddened these stars using the $J-H$ color-magnitude diagram adopting the 1 Myr isochrone (Meyer 1996; Carpenter et al. 1997; Wilking et al. 2004).

4. ANALYSIS

In this section we use the *HST* photometry to constrain the stellar and substellar IMF in the central part of the Mon R2 cluster, as well as revisit the fraction of stellar mass objects with circumstellar disks. We begin by first defining an extinction-limited sample that is complete down to 0.1 $M_\odot$. We use this sample to determine the fraction of stars with circumstellar disks and to search for variations in the extinction as a function of object mass. We then define three extinction-limited samples complete for both stars and brown dwarfs in order to constrain the substellar IMF of Mon R2 and compare these ratios with the field star IMF and other star-forming regions.

4.1. *The Circumstellar Disk Fraction for Stars in Mon R2*

What is the fraction of stellar objects in our extinction-limited sample showing evidence for a circumstellar disk, as discussed above? We have constructed an extinction-limited sample in order to obtain a representative sample across the whole mass range considered. Without an extinction-limited sample, we would underestimate the number of fainter, lower mass sources relative to intrinsically more luminous objects of higher mass. The maximum extinction is determined such that the sample considered will be complete down to spectral type M6, corresponding to a 0.1 $M_\odot$ star for the 1 Myr isochrone. This corresponds to an extinction limit of $A_V = 19$ mag. We have excluded the two objects on the blue side of the isochrone in Figure 4, since these objects are probable foreground stars (stars 61 and 83). Exclusion of these objects is equivalent to excluding objects with a derived extinction less than $A_V = 1$ mag. The extinction-limited sample ($A_V = 19$ mag) contains 43 objects in total. The selected sources are all located between the two upper dashed lines in Figure 4. In § 4.2 we construct three further extinction-limited samples in order to address the IMF into the brown dwarf regime.

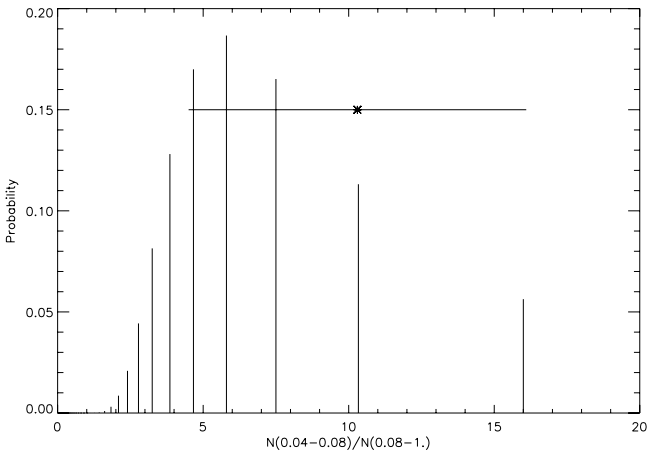

FIG. 6.—Comparison of our derived R value with the R values obtained from a Chabrier (2003) field IMF for a sample size of 34 objects. The predicted ratio distribution from the field IMF was determined using the binomial distribution.

For objects with a mass between 0.1 and 1.0 $M_\odot$, we find a disk fraction of 27% ± 9%. For a wider area but more shallow survey of Mon R2, Carpenter et al. (1997) found a disk fraction of 48% ± 8% from *JHK* photometry. A disk fraction of ~30% is relatively low compared to what is found in other star clusters of comparable age. For example, in the ONC, Lada et al. (2000) found a disk fraction of 50% ± 20% using *JHK* photometry (e.g., Hillenbrand et al. 1998), which within the error bars is consistent with Mon R2. Haisch et al. (2001) found a disk fraction of 21% ± 5% in IC 348 using *JHK* photometry.

4.2. *Constraints on the IMF in the Center of Mon R2*

With a data set significantly deeper than the previous study by Carpenter et al. (1997) we can constrain the IMF into the brown dwarf regime. The use of an extinction-limited sample for IMF studies assumes that the extinction distribution is independent of the object's mass. If this is not the case, a bias would be introduced by preferentially excluding either high- or low-mass objects. To test whether the extinction distribution is independent of object mass, we have divided our sample into objects between 0.2 and 1 $M_\odot$ and between 0.03 and 0.2 $M_\odot$ for an $A_V \leq 10$ mag extinction-limited sample (see below). We have then performed a two-sided Kolmogorov-Smirnov (K-S) test of whether the extinction distributions are consistent with having been drawn from the same parent population. The K-S test returned a value of 0.49, from which we conclude that there is no obvious difference in the extinction distribution as a function of mass.

We have calculated the ratio of stars between 0.08 and 1 $M_\odot$ divided by the number of objects between 0.04 and 0.08 $M_\odot$, $R = N(0.08\text{–}1.0\ M_\odot)/N(0.04\text{–}0.08\ M_\odot)$, for an extinction-limited sample, $A_V \leq 13$ mag, based on 34 objects. The ratio is found to be $R = 10.3 \pm 5.8$ for a cluster age of 1 Myr, where the errors are derived assuming Poisson errors. We then compared the ratio with the similar predicted ratio from the Chabrier (2003) system field star IMF ($dN/d\log M \propto \exp\left[-(\log m - \log 0.22)^2/(2 \times 0.57^2)\right]$). The distribution of predicted ratios is given by the binomial distribution and is shown in Figure 6. The height of each line shows the probability of a given ratio.

Although the ratio derived for Mon R2 is slightly higher than the peak of the distribution of ratios predicted by the Chabrier (2003) system IMF, the probability of obtaining the derived value or higher from the Chabrier system IMF is 19%.

We have constructed two additional extinction-limited samples, one down to $A_V = 10$ mag and one down to $A_V = 7$ mag. The two samples are complete down to $30M_J$ and $20M_J$, respectively. The upper mass for both samples is still 1 $M_\odot$. Although both samples extend to fainter absolute magnitudes than the $A_V = 13$ mag sample, the lower maximum extinction reduces the sample sizes significantly. Only 19 objects are included in the $A_V = 10$ mag sample and 13 in the $A_V = 7$ mag sample. We have calculated the ratio of high-mass to low-mass objects for the two latter samples in a manner similar to that above. We find the ratios $R^* = N(0.08\text{–}1.0\ M_\odot)/N(0.03\text{–}0.08\ M_\odot) = 8.5 \pm 6.4$ and $R^{**} = N(0.08\text{–}1.0\ M_\odot)/N(0.02\text{–}0.08\ M_\odot) = 2.2 \pm 1.3$. The similar expected ratios from the Chabrier (2003) system IMF are $R^* = 4.2$ and $R^{**} = 3.5$, respectively. It appears that the ratio of stars to brown dwarfs observed relative to the ratio expected from Chabrier (2003) decreases ($R = 10.3 \pm 5.8$ vs. 5.3; $R^* = 8.5 \pm 6.4$ vs. 4.3; $R^{**} = 2.2 \pm 1.3$ vs. 3.5) as a function of depth into the cloud. If confirmed, this might suggest that brown dwarfs and stars are not uniformly distributed in Mon R2. However, the K-S test did not indicate that the distribution of extinction is different for the high- and low-mass samples, down to 0.03 $M_\odot$, so we do not believe these differences to be significant. All the observed ratios are consistent with the Chabrier (2003) IMF. The cumulative distributions of the absolute J-band magnitudes for the three extinction-limited samples are shown in Figure 7. The location of a 0.08 $M_\odot$ 1 Myr object from the Baraffe et al. (1998) models is indicated.

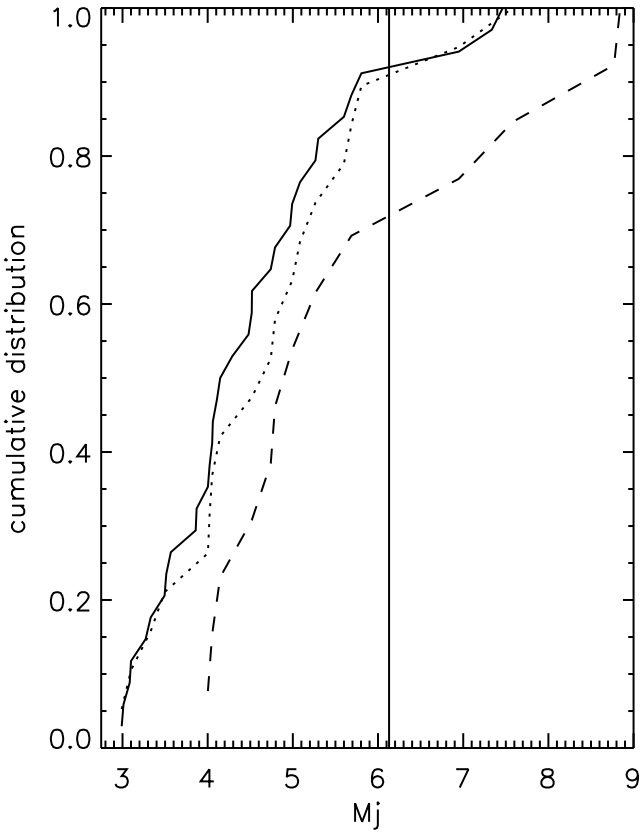

FIG. 7.—Cumulative distributions of the absolute J-band magnitudes for the objects in the three extinction-limited samples, $A_V = 13$ mag (*solid line*, 34 objects), $A_V = 10$ mag (*dotted line*, 19 objects), and $A_V = 7$ mag (*dashed line*, 13 objects). The absolute magnitude of a 1 Myr, 0.08 $M_\odot$ object (Baraffe et al. 1998) is marked by the vertical solid line.

5. DISCUSSION

The derived ratios of high-mass to low-mass objects can be compared with similar ratios derived from other young star clusters with similar spatial resolution. We focus here on some of the

TABLE 5
DERIVED RATIOS

Ratio	M_{low}	Mon R2	Field[a]	Field[b]	IC 348[c]	Taurus[d]	ONC[e]	ONC[f]
R	0.04	10.3 ± 5.8	2.9	5.3	16.8 ± 5.8	9.6 ± 3.2	6.4	5.5 ± 0.8
R^*	0.03	8.5 ± 6.4	2.2	4.2	11.6 ± 3.4	6.9 ± 2.0	4.7	4.3 ± 0.6
R^{**}	0.02	2.2 ± 1.3	1.7	3.5	...	5.4 ± 1.4	3.7	3.0 ± 0.6

NOTE.—Derived ratios of high-mass to low-mass objects for Mon R2, the field star IMF, and other star-forming regions.
[a] Kroupa (2002) single-star IMF.
[b] Chabrier (2003) system IMF.
[c] Luhman et al. (2003).
[d] Luhman (2004).
[e] Muench et al. (2002).
[f] Hillenbrand & Carpenter (2000).

best-studied clusters, namely, the ONC, IC 348, and Taurus, and compare the values of R, R^*, and R^{**} for those clusters with the values derived here. We briefly discuss the selection criteria for the IMF samples for the different clusters, and we compile the ratios in Table 5.

As the closest site of massive star formation, the ONC has been observed in some detail. The IMF has been estimated through deep near-infrared imaging (Hillenbrand & Carpenter 2000; Muench et al. 2002). Using H- and K-band observations, Hillenbrand & Carpenter (2000) derived the IMF down to $0.02\,M_\odot$ for $A_V \leq 10$ mag. From their histogram we have derived the ratios for the ONC, where we find $R = 5.5 \pm 0.8$, $R^* = 4.3 \pm 0.6$, and $R^{**} = 3.0 \pm 0.6$. In another imaging study, the IMF of the ONC was constrained through model fits to the K-band luminosity function by Muench et al. (2002) down to $\sim 10 M_J$. The ratio of stars to brown dwarfs was found by integrating the functional fit to the IMF presented by Muench et al. (2002). From the functional fit, we find $R = 6.4$, $R^* = 4.7$, and $R^{**} = 3.7$, consistent with both the result of Hillenbrand & Carpenter (2000) and our ratios for Mon R2.

Spectroscopic observations of objects in the ONC by Slesnick et al. (2004) indicate that the ratio of high-mass to low-mass objects might be higher than found from imaging alone. A ratio of $R' = N(0.08\text{–}0.4\ M_\odot)/N(0.03\text{–}0.08\,M_\odot) = 4.5 \pm 0.7$ is found from the spectroscopic survey. It should be kept in mind that correction factors of ~ 2 have been applied to the number counts, as discussed in Slesnick et al. (2004). The comparable ratio for Mon R2 is 4.5 ± 3.5, which is in excellent agreement with the Slesnick et al. (2004) result. For comparison, the similar ratio from the Muench et al. (2002) IMF is 4.1.

As one of the nearest low-mass star-forming regions to the Sun, Taurus has been investigated in detail. Luhman (2004) has presented the IMF down to $0.015\ M_\odot$ for an extinction-limited sample at $A_V \leq 4$ mag. We have calculated the ratio of high- to low-mass stars from the data presented by Luhman (2004). We find the derived IMFs for Taurus and Mon R2 to be consistent within the uncertainties for all three ratios.

The ratios for Taurus might be suspect for two reasons. Luhman (2004) emphasized that the sample is incomplete for the mass interval $0.3\text{–}0.6\ M_\odot$ due to saturation, resulting in the derived ratios being lower limits. Also, the surveyed region by Luhman (2004) only covered parts of Taurus (4 deg^2) preferentially centered on the dense filaments. A larger area survey (28 deg^2) has found relatively more brown dwarfs (Guieu et al. 2006), although the latter survey only extended down to $0.03\ M_\odot$, for an extinction-limited sample at $A_V \leq 4$ mag. They concluded that the ratios of brown dwarfs to stars in Taurus and the ONC are similar within the statistical uncertainties. Although the ratio derived by Guieu et al. (2006) extended to higher masses relative to this paper, we can still estimate the effect of their updated number of brown dwarfs in Taurus. The newly detected brown dwarfs in the larger region surveyed by Guieu et al. (2006) reduced the derived ratios by $\sim 25\%$ relative to Luhman (2004). Correcting the Taurus results quoted in Table 5 downward by 25% only improves the agreement with the ratios for Mon R2.

The low-mass stellar content of IC 348 has been investigated recently by Luhman et al. (2003). The IMF was derived down to $30 M_J$, using an extinction-limited sample at $A_V \leq 4$ mag. The objects presented by Luhman et al. (2003) have been spectroscopically confirmed as members. The spatial resolution in the imaging survey was $0\farcs6$. Scaled to the distance of Mon R2, this is a similar physical resolution to that in our F207M-band image. Based on the data published in Luhman (2004) we have derived the ratios $R = 16.8 \pm 5.8$ and $R^* = 11.6 \pm 3.3$. The ratios for IC 348 appear to be relatively high but still consistent within $2\,\sigma$ with the results for Mon R2. The IMF has been probed in IC 348 down to $0.015\ M_\odot$ using *HST* NICMOS2 imaging (Najita et al. 2000). Using the strength of the 1.9 μm water band, they determined the spectral type of objects in the mass interval 0.015–$0.7\ M_\odot$. We have calculated the modified ratio of high-mass to low-mass objects using objects between 0.25 and $0.7\ M_\odot$ as the high-mass objects and 0.02 and $0.25\ M_\odot$ as the low-mass objects. The ratio derived from the histogram in Najita et al. (2000) is 0.4, whereas the similar ratio for Mon R2 is 0.3 ± 0.2 for an extinction-limited sample, $A_V \leq 7$ mag.

One issue that should be explicitly taken into account in these comparisons is the role of binaries. It is well known that a large fraction of stars reside in multiple systems, and due to our finite angular resolution, we can only resolve a certain fraction of the binary systems in each cluster. The resolution in the F207M band with *HST* NICMOS2 at a distance of 830 pc resolves all systems more widely separated than ~ 160 AU. Both of the ONC imaging surveys have a physical resolution similar to that of this study. Luhman (2004) considered all objects with a separation smaller than $2''$ in Taurus as single objects. For a distance of 140 pc, this corresponds to a separation of 280 AU. On the other hand, the *HST* NICMOS2 imaging of IC 348 by Najita et al. (2000) has twice the physical resolution as this study, resolving binaries with separation larger than ~ 75 AU. Since the physical angular resolution is similar to within a factor of ~ 2 for most of the clusters compared, we do not expect unresolved binaries to affect the ratios differently for the clusters discussed here. However, the field IMF by Kroupa (2002) has been constructed from individual objects. The majority of binaries in young open clusters have separations smaller than ~ 100 AU (Patience et al. 2002; e.g., Duquennoy & Mayor 1991) and would be unresolvable in our observations. The quantitative change of the IMF due to unresolved binaries depends on the details of the binary frequency

versus separation and the distribution of mass ratios, neither of which are well known, especially for low masses. However, there is some indication that the binary frequency is lower for cool objects (Burgasser et al. 2006). Chabrier (2003) have presented the system IMF assuming no unresolved binaries derived from the local 8 pc solar neighborhood field star sample, which is used in Table 5.

The derived ratios for Mon R2 appear consistent with the similar ratios for the ONC, IC 348, and Taurus. They are also consistent with the ratios derived for both the Kroupa (2002) and Chabrier (2003) IMF. Thus, despite more than an order of magnitude difference in total cluster mass, it appears that the IMF down to 0.02 $M_\odot$ is similar. *So far, there is little evidence for variations in the substellar IMF, at least down to 20M_J.* It remains to be seen whether the ensemble of the observations can distinguish between a flat and a falling IMF between 0.02 and 0.08 $M_\odot$ (e.g., Allen et al. 2005).

Several theoretical considerations would predict a deficit of brown dwarfs in Taurus relative to more massive regions. Goodwin et al. (2004a) suggest the IMF in a region like Taurus should have relatively fewer brown dwarfs due to the narrow distribution of core masses in Taurus relative to regions like the ONC. An alternative explanation has been presented by Bate & Bonnell (2005). They suggested the lower density in the Taurus molecular cores results in a higher Jeans mass, which in turns results in a higher average mass. Goodwin et al. (2004b) indicate through numerical simulations that the peak of the IMF will shift to lower masses as the degree of turbulence increases.

The increase of the relative number of brown dwarfs in Mon R2 when the minimum mass of the sample is decreased is curious. Since the extinction limit decreases as the limiting mass is extended to lower masses, one possibility is that the more massive stars are observed preferentially deeper within the molecular cloud. However, we found no evidence for variation in the extinction as a function of object mass down to 0.03 $M_\odot$. One possibility, although speculative, is that the brown dwarfs have been ejected from small *N*-body systems as proposed by, e.g., Reipurth & Clarke (2001). We would then detect the brown dwarfs ejected toward us (preferentially with lower extinction) even though the parent system containing the star would be located deeper in the cloud. Since we are only probing the surface of the cluster in the most shallow extinction-limited samples, such a scenario would explain the observed trend. Deeper analysis of the dynamical evolution (velocities and spatial distribution) of cluster members as a function of mass is needed.

6. CONCLUSIONS

We have presented the results from *HST* NICMOS2 F110W-, F160W-, F165M-, and F207M-band imaging of the inner $1' \times 1'$ of the embedded cluster associated with Mon R2. Our results are as follows:

1. The effective temperature has been estimated for a small set of stars in the temperature range 2700–3300 K based on a water vapor index, and these objects have been placed in the H-R diagram. A 1 Myr Baraffe et al. (1998) isochrone is consistent with the lower mass objects placed in the H-R diagram, in agreement with Carpenter et al. (1997).

2. We find, for stars with spectral type M6 or earlier (0.1–1 $M_\odot$), a disk fraction of 27% ± 9% based on an extinction-limited sample of 43 stars at $A_V \leq 19$ mag.

3. We create three extinction-limited samples complete for $A_V = 13$, 10, and 7 mag and containing 34, 19, and 13 objects, respectively. We have calculated the three ratios of low-mass stars to brown dwarfs: $R = N(0.08\text{–}1.0\ M_\odot)/(0.04\text{–}0.08\ M_\odot) = 10.3 \pm 5.8$, $R^* = N(0.08\text{–}1.0\ M_\odot)/N(0.03\text{–}0.08\ M_\odot) = 8.5 \pm 6.4$, and $R^{**} = N(0.08\text{–}1.0\ M_\odot)/N(0.02\text{–}0.08\ M_\odot) = 2.2 \pm 1.3$.

4. The derived ratios are consistent with the similar ratios for Taurus, IC 348, the ONC, and the system field IMF of Chabrier (2003). Thus, there is no compelling evidence for variations in the relative brown dwarf content between Mon R2 and other nearby star-forming regions.

This paper is based on observations made with the NASA/ESA *Hubble Space Telescope*, operated by the Space Telescope Science Institute, which is operated by the Association of Universities for Research in Astronomy, Inc., under NASA contract NAS5-26555. This work was supported by a Cottrell Scholar's Award to M. R. M. from the Research Corporation and NASA grant HST13-9846. We would like to thank Catherine Slesnick and Lynne Hillenbrand for providing the data from their spectroscopic survey of the ONC. We thank Steve Strom for discussions during the early stages of the project, France Allard for assistance with the models, Erick Young and Hua Chen for help in preparations of the observations, Angela Cotera for advice concerning the image processing, and Kevin Luhman for assistance in calculating the mass ratios for IC 348 and Taurus. We also thank the referee, August Muench, for comments and suggestions that improved and clarified the paper.

REFERENCES

Allard, F., Hauschildt, P. H., & Schweitzer, A. 2000, ApJ, 539, 366
Allen, P. R., Koerner, D. W., Reid, I. N., & Trilling, D. E. 2005, ApJ, 625, 385
Baraffe, I., Chabrier, G., Allard, F., & Hauschildt, P. H. 1998, A&A, 337, 403
Bate, M. R., & Bonnell, I. A. 2005, MNRAS, 356, 1201
Beckwith, S., Evans, N. J., Becklin, E. E., & Neugebauer, G. 1976, ApJ, 208, 390
Bessell, M. S. 1991, AJ, 101, 662
Bessell, M. S., & Brett, J. M. 1988, PASP, 100, 1134
Briceño, C., Luhman, K. L., Hartmann, L., Stauffer, J. R., & Kirkpatrick, J. D. 2002, ApJ, 580, 317
Burgasser, A. J., Reid, I. N., Siegler, N., Close, L., Allen, P., Lowrance, P., & Gizis, J. 2006, in Protostars and Planets V, in press
Carpenter, J. M., Meyer, M. R., Dougados, C., Strom, S. E., & Hillenbrand, L. A. 1997, AJ, 114, 198
Chabrier, G. 2003, PASP, 115, 763
Choi, M., Evans, N. J., Tafalla, M., & Bachiller, R. 2000, ApJ, 538, 738
Dahn, C. C., et al. 2002, AJ, 124, 1170
Duquennoy, A., & Mayor, M. 1991, A&A, 248, 485
Goodwin, S. P., Whitworth, A. P., & Ward-Thompson, D. 2004a, A&A, 419, 543
Goodwin, S. P., Whitworth, A. P., & Ward-Thompson, D. 2004b, A&A, 423, 169
Gorlova, N. I., Meyer, M. R., Rieke, G. H., & Liebert, J. 2003, ApJ, 593, 1074
Guieu, S., Dougados, C., Monin, J.-L., Magnier, E., & Martín, E. L. 2006, A&A, 446, 485
Haisch, K. E., Lada, E. A., & Lada, C. J. 2001, AJ, 121, 2065
Hauschildt, P. H., Allard, F., & Baron, E. 1999, ApJ, 512, 377
Herbst, W., & Racine, R. 1976, AJ, 81, 840
Hillenbrand, L. A., & Carpenter, J. M. 2000, ApJ, 540, 236
Hillenbrand, L. A., & Hartmann, L. W. 1998, ApJ, 492, 540
Hillenbrand, L. A., Strom, S. E., Calvet, N., Merrill, K. M., Gatley, I., Makidon, R. B., Meyer, M. R., & Skrutskie, M. F. 1998, AJ, 116, 1816
Krist, J. E., Golimowski, D. A., Schroeder, D. J., & Henry, T. J. 1998, PASP, 110, 1046
Kroupa, P. 2002, Science, 295, 82
Lada, C. J., Muench, A. A., Haisch, K. E., Lada, E. A., Alves, J. F., Tollestrup, E. V., & Willner, S. P. 2000, AJ, 120, 3162
Leggett, S. K., Allard, F., Berriman, G., Dahn, C. C., & Hauschildt, P. H. 1996, ApJS, 104, 117
Lehár, J., et al. 2000, ApJ, 536, 584
Luhman, K. L. 2004, ApJ, 617, 1216

Luhman, K. L., Stauffer, J. R., Muench, A. A., Rieke, G. H., Lada, E. A., Bouvier, J., & Lada, C. J. 2003, ApJ, 593, 1093
Massi, M., Felli, M., & Simon, M. 1985, A&A, 152, 387
Meyer, M. R. 1996, Ph.D. thesis, Univ. Massachusetts
Meyer, M. R., Adams, F. C., Hillenbrand, L. A., Carpenter, J. M., & Larson, R. B. 2000, in Protostars and Planets IV, ed. V. Mannings, A. P. Boss, & S. S. Russell (Tucson: Univ. Arizona Press), 121
Meyer, M. R., Calvet, N., & Hillenbrand, L. A. 1997, AJ, 114, 288
Miller, G. E., & Scalo, J. M. 1979, ApJS, 41, 513
Muench, A. A., Lada, E. A., Lada, C. J., & Alves, J. 2002, ApJ, 573, 366
Najita, J. R., Tiede, G. P., & Carr, J. S. 2000, ApJ, 541, 977
Onishi, T., Mizuno, A., Kawamura, A., Tachihara, K., & Fukui, Y. 2002, ApJ, 575, 950
Palla, F., & Stahler, S. W. 1999, ApJ, 525, 772
Patience, J., Ghez, A. M., Reid, I. N., & Matthews, K. 2002, AJ, 123, 1570
Reipurth, B., & Clarke, C. 2001, AJ, 122, 432
Robin, A. C., Reylé, C., Derrière, S., & Picaud, S. 2003, A&A, 409, 523
Schmidt-Kaler, Th. 1982, Landolt-Bornstein: Numerical Data and Functional Relationships in Science and Technology (Berlin: Springer)
Slesnick, C. L., Hillenbrand, L. A., & Carpenter, J. M. 2004, ApJ, 610, 1045
Wilking, B. A., Meyer, M. R., Greene, T. P., Mikhail, A., & Carlson, G. 2004, AJ, 127, 1131